PAST KNOWLEDGE PEOPLE

ISSN: 2994-6433

Research Article

Journal of Sensor Networks and Data Communications

Orthogonal-Projection Localization for Polar Sensing Systems

Greg Passmore*

PassmoreLab, Austin, Texas, USA

***Corresponding Author**
Greg Passmore, PassmoreLab, Austin, Texas, USA.

Submitted: 2025, Oct 01; **Accepted**: 2025, Dec 01; **Published**: 2025, Dec 15

Citation: Passmore, G. (2025). Orthogonal-Projection Localization for Polar Sensing Systems. *J Sen Net Data Comm, 5*(3), 01-10.

Abstract

The geometry of polar sensing systems contains sufficient information to reveal the position of the emitter or receiver that produced the data. Each beam or return defines a directional path between its near and far samples, and the intersection of these paths identifies the origin from which the energy was transmitted or received. This point is found by minimizing the summed orthogonal distances between a candidate origin and all ray directions, a relationship that emerges naturally from the spatial arrangement of the data. The same structure is present in radar, LiDAR, and sonar observations, where energy follows radial trajectories through a common geometric framework. The process also applies to hidden or non-cooperative emitters detected only through intermediate reflections or interference patterns, where indirect observations carry sufficient directional evidence to infer the source position. When timing, Doppler, or received-power information is available, these can be incorporated as natural weighting terms within the same least squares balance. The result exposes an underlying geometric law that links measured returns, their directional vectors, and the origin implied by their geometric intersection.

Keywords: Emitter localization, Least-squares intersection, Polar sensing, LiDAR, Radar, Sonar, Backscatter, Geometric reconstruction, Direction vectors, Spatial equilibrium

1. The Problem

Polar sensing measurements record where transmitted energy interacts with a surface, but often omit the position from which that energy originated. Many data formats, such as PTS or ASC, list only the three-dimensional coordinates of the returns without including the sensor's location or orientation. When such points exist in a shared coordinate frame, their spatial organization can still disclose the origin implied by the scan geometry. Each scanline or beam defines a radial path, and together these paths converge toward the point of emission. This same relationship governs optical, radar, and acoustic systems, which all measure reflections along straight or refracted radial directions. Even when the emitter itself is hidden, behind terrain, underwater features, or within clutter, its position can be inferred from backscatter observed by another platform. Each reflection provides a directional constraint toward the source, and the collective balance of these constraints reveals the origin already contained within the geometry of the observations. The same geometric relationship can also be seen in interference mapping and jammer localization, where bearings and signal gradients converge through the least-squares intersection to indicate the position implied by the spatial structure of the observations.

2. Prior Work

Estimating an unknown origin from directional data has appeared in several forms across imaging, radar, and acoustic research. The classical image-triangulation problem provides an early example. Hartley and Sturm (1997) examined the intersection of noisy image rays and derived least-squares solutions for point reconstruction from multiple views. Their analysis, later expanded by Hartley and Zisserman (2004), established the basis for geometric reconstruction by minimizing orthogonal distances between rays in three-dimensional space. Kanatani, Sugaya, and Niitsuma (2008) extended this work by introducing algebraic corrections and stability analysis, emphasizing robustness when the rays are nearly parallel or poorly conditioned. These studies reveal the same underlying mathematical structure present in the current formulation, though developed within the context of optical imaging geometry.

A separate line of research addresses emitter localization from range or timing information. Foy (1976) and Chan and Ho (1994) described both iterative and closed-form solutions for time-difference-of-arrival (TDOA) systems, in which hyperbolic range-difference constraints define the feasible region of the source. The relationship identified here differs in that it originates from directional rather than temporal data, yet the timing terms appear naturally as additional constraints within the same least-squares projection framework. In this sense, range-difference geometry represents another expression of the same spatial balance.

Bearings-only tracking studies also express this geometry. Nardone and Aidala (1981) analyzed observability and convergence properties for bearings-only localization, showing that geometry and relative motion determine when a unique solution can exist. Farina (1999) later summarized these and related approaches in a comprehensive treatment of passive tracking. The present method differs by using the projector form $P_i = I - d_i d_i^\top$, which aggregates all bearing constraints into a single symmetric system $A\hat{p} = b$ without requiring temporal sequencing or filter-based motion modeling. This makes it suitable for both static datasets and streaming updates.

Mathematically, the least-squares intersection relates to the "closest point to many lines" problem discussed in geometric optimization literature (Strang, 1986; Trefethen and Bau, 1997). However, the current treatment emphasizes the geometric balance revealed by the projection operators rather than the solver itself. Each term represents a component of the equilibrium already inherent in the data, and the intersection point represents the origin implied by the collective directions, independent of platform metadata or sensing type.

3. Recovering Sensor Origin from Structured Scanlines

Polar datasets typically contain only sampled return positions without explicit metadata identifying the emitter or receiver origin. These datasets may already be globally aligned, yet without the origin position it is not possible to reconstruct the true propagation geometry. The method estimates the origin *p* from the point set itself by using the natural ray structure implied by each scanline. Each scanline defines a near–far pair of points that form a directional vector along which energy was transmitted or received. The least-squares intersection of all such lines yields an estimate of the sensor origin in the same coordinate frame as the data.

4. Importance of Sensor Origin

The sensor origin defines the direction of incidence for each recorded point, enabling computation of surface normals that face the sensor and determination of front, versus back-facing surfaces. The origin establishes energy propagation direction and is required to model beam divergence and footprint growth with range, which influence apparent roughness, intensity, and backscatter strength. Line-of-sight and shadow analysis depend on the origin for visibility tests and path-length modeling. Intensity normalization, backscatter modeling, and multi-return simulation require incidence angle and range referenced to the origin. In multi-scan or multi-sensor datasets, per-scan origin recovery enables angular incidence mapping, reflectivity corrections, exposure modeling, and verification of inter-scan alignment across radar, LiDAR, and sonar modalities.

5. Data Model

An organized point set is divided into vertical columns of width *W* and height *H*. For each column *c*, the first finite point a_i and the last finite point b_i define a line segment. The normalized direction vector is

$$d_i = \frac{b_i - a_i}{\|b_i - a_i\|}$$

Columns with invalid or degenerate pairs are excluded.

6. Finding Matrix Dimensions

A user may have to infer grid dimensions from a sequential point list using inter-point jumps. A sequential export of an organized scan typically traverses samples column-by-column. In column-major order, successive points within a column are spatially adjacent, while the transition from the last point of one column to the first point of the next produces a larger spatial jump. Let the ordered samples be $\{x_i\}_{i=1}^{n}$, $x_i \in \mathbb{R}^3$. Define successive Euclidean gaps

$$\Delta_i = \|x_{i+1} - x_i\| \quad \text{for } i = 1, \ldots, n-1.$$

Within a column, Δ_i remains small due to local surface continuity. At a column boundary, Δ_i is typically much larger because the path moves from the far end of one scan-line to the near start of the next. A robust threshold τ distinguishes within-column steps from cross-column jumps. Using the median absolute deviation (MAD), let

$$m = \text{median}(\{\Delta_i\}), \qquad \text{MAD} = \text{median}(|\Delta_i - m|), \qquad \tau = m + k \cdot \text{MAD},$$

with $k \in [6,12]$ for typical terrestrial data. Indices with $\Delta_i > \tau$ mark boundaries. The sequence is partitioned into contiguous runs $\mathcal{R}_j$ of lengths L_j, each run corresponding to a column. The grid height is estimated as the statistical mode of the run lengths,

$$\widehat{H} = \text{mode}\{L_j\},$$

and the grid width as

$$\widehat{W} = \left\lfloor \frac{n}{\widehat{H}} \right\rceil,$$

rounded to the nearest integer. Outlier runs caused by occlusions or missing data are rejected by retaining lengths within a tolerance band around $\widehat{H}$, for example $|L_j - \widehat{H}| \le \epsilon$ with $\epsilon \in \{1, 2\}$.

6.1. Using Nearest–Farthest Depth Ordering Within Each Run

Let a run $\mathcal{R}_j = \{x_{s(j)}, \ldots, x_{e(j)}\}$ be one column. Define a surrogate depth along the column by cumulative chord length:

$$u_{s(j)} = 0, \qquad u_{i+1} = u_i + \|x_{i+1} - x_i\| \quad \text{for } i \in [s(j), e(j) - 1].$$

If samples are ordered near-to-far, u is strictly increasing and the first and last valid points in $\mathcal{R}_j$ provide (a_j, b_j) for ray formation. If the device writes far-to-near, the same holds with reversed orientation. The inter-run jump at $e(j)$ resets u at the start of $\mathcal{R}_{j+1}$, validating near–far identification without prior knowledge of p.

6.2. PCA Check to Confirm Columnarity

Compute the run covariance

$$C_j = \frac{1}{L_j} \sum_{i=s(j)}^{e(j)} (x_i - \bar{x}_j)(x_i - \bar{x}_j)^\top, \qquad \bar{x}_j = \frac{1}{L_j} \sum_{i=s(j)}^{e(j)} x_i.$$

Let $\lambda_{1,j} \ge \lambda_{2,j} \ge \lambda_{3,j}$ be eigenvalues. A well-formed column exhibits a strong one-dimensional structure quantified by

$$\rho_j = \frac{\lambda_{1,j}}{\lambda_{2,j} + \lambda_{3,j}},$$

with $\rho_j \gg 1$. Runs failing a minimum ρ_j are discarded, and $\widehat{H}, \widehat{W}$ are recomputed from the filtered runs.

6.3. Nearest–Farthest Extremes as a Consistency Test

Using the run's principal direction $\hat{d}_j$ (eigenvector of $\lambda_{1,j}$), define $t_i = \hat{d}_j^\top (x_i - \bar{x}_j)$. The ordered pair (min ti, max ti) should occur near the run endpoints, providing a near–far orientation cue. Grid dimensions remain determined by run lengths, and (a_j, b_j) are taken as the first and last valid points.

7. Scanner Location Using Geometric Basis

The orthogonal distance from p to line (a_i, d_i) is represented as

$$r_i(p) = P_i(p - a_i)$$

with projection matrix

$$P_i = I - d_i d_i^\top.$$

The least-squares objective is

$$J(p) = \sum_i \|r_i(p)\|^2 = \sum_i (p - a_i)^\top P_i (p - a_i).$$

Setting the gradient to zero gives

$$\sum_i P_i (p - a_i) = 0,$$

or equivalently

$$Ap = b,$$

with

$$A = \sum_i P_i, \qquad b = \sum_i P_i a_i.$$

7.1. Matrix Structure

Each P_i expands to

$$P_i = \begin{bmatrix} 1 - d_x^2 & -d_x d_y & -d_x d_z \\ -d_y d_x & 1 - d_y^2 & -d_y d_z \\ -d_z d_x & -d_z d_y & 1 - d_z^2 \end{bmatrix}.$$

The matrix A is symmetric and positive semidefinite. A unique solution requires sufficient diversity in the $\{d_i\}$ directions.

7.2. Closed-Form Solution

Using the symmetric entries A_{00}, A_{01}, A_{02}, A_{11}, A_{12}, A_{22}, the determinant is

$$\det(A) = A_{00}(A_{11}A_{22} - A_{12}^2) - A_{01}(A_{01}A_{22} - A_{12}A_{02}) + A_{02}(A_{01}A_{12} - A_{11}A_{02}).$$

The adjugate elements are

$$C_{00} = A_{11}A_{22} - A_{12}^2, \quad C_{01} = -(A_{01}A_{22} - A_{12}A_{02}), \quad C_{02} = A_{01}A_{12} - A_{11}A_{02},$$

$$C_{11} = A_{00}A_{22} - A_{02}^2, \quad C_{12} = -(A_{00}A_{12} - A_{01}A_{02}), \quad C_{22} = A_{00}A_{11} - A_{01}^2.$$

The inverse is

$$A^{-1} = \frac{1}{\det(A)} \begin{bmatrix} C_{00} & C_{01} & C_{02} \\ C_{01} & C_{11} & C_{12} \\ C_{02} & C_{12} & C_{22} \end{bmatrix},$$

and the solution is $p = A^{-1}b$.

7.3. Implementation Notes

Accumulate the six unique entries of A and the three entries of b. Use double precision for accumulation. Apply a determinant threshold to detect degeneracy. When directional diversity is weak, return NaNs.

7.4. Weighting Extension

Introduce nonnegative weights w_i to reflect confidence, line length, or variance:

$$\Big(\sum_i w_i P_i\Big) p = \sum_i w_i P_i a_i.$$

7.5. Uncertainty Estimate

Assuming isotropic residual covariance $\sigma^2 I$ at the projector outputs, approximate

$$\mathrm{Cov}(p) \approx \sigma^2 (A^\top A)^{-1},$$

and estimate $\hat{\sigma}^2$ from residuals

$$\hat{\sigma}^2 = \frac{1}{\max(1, n_c - 3)} \sum_i \|P_i(\hat{p} - a_i)\|^2,$$

where n_c is the number of contributing rays.

7.6. Numerical Behavior

Degeneracy occurs when most d_i are nearly parallel. Use conditioning checks on A, optionally an adaptive rule such as declaring failure when $\det(A) < \epsilon \|A\|_F^3$ with $\epsilon \approx 10^{-10}$.

8. Application to Radar, Sonar, and Other Polar Modalities

The geometric principle extends to radar, sonar, and optical time-of-flight systems. For a steering direction d_i and one or more ranges $r_{i,k}$ along that direction, return points satisfy

$$x_{i,k} = p + r_{i,k} d_i.$$

When p is unknown but $\{x_{i,k}\}$ are embedded in a common frame, rays are formed using $a_i = x_{i,\,\min}$ and $b_i = x_{i,\max}$ and the same least-squares intersection is solved. The method applies to monostatic and bistatic configurations when the relevant ray directions are known or inferable.

Polar beams traverse layered media and reflect from intermediate and distant surfaces. Recovering p separates geometric propagation from environmental effects, enabling calculation of incidence angles, slant-range corrections, footprint size under beam divergence, multi-path discrimination via residual analysis, and energy loss modeling where attenuation and phase depend on path length and angle relative to the origin. When datasets are georeferenced or fused into a global frame, recovering p anchors local coordinate frames, supports Doppler–angle correlation, and calibrates directional response. The approach remains useful when metadata are absent or restricted while geometric relationships persist in the data.

9. Hidden Emitter Localization by Least-Squares Intersection

Hidden emitter localization relies on reconstructing the emission geometry of a LiDAR or electromagnetic source from indirect or secondary measurements. The least-squares intersection method estimates the origin $\hat{p}$ by minimizing the squared perpendicular distances between the hypothesized source and all observed propagation rays. The governing normal equations are

$$A\hat{p} = b,$$

where

$$A = \sum_{i=1}^{N} (I - d_i d_i^\top), \quad b = \sum_{i=1}^{N} (I - d_i d_i^\top) a_i.$$

Here, N is the total number of available observations, a_i is the known anchor position (reflection, phase center, or aperture element), and d_i is the corresponding unit direction vector. Each term $(I - d_i d_i^\top)$ acts as a projection operator removing the component of $(\hat{p} - a_i)$ parallel to d_i. The estimated position $\hat{p}$ minimizes the total squared projection residuals:

$$\hat{p} = \arg\min_{p} \sum_{i=1}^{N} \| (I - d_i d_i^\top)(p - a_i) \|^2.$$

The following subsections describe how a_i and d_i are derived from different observation modalities.

9.1. Backscatter Geometry

When secondary radar or LiDAR detects energy reflected from intermediate surfaces, each return defines an observation at position a_i with an inferred direction d_i. These vectors represent approximate ray paths from the hidden emitter. The residual for each observation is

$$r_i = (I - d_i d_i^\top)(\hat{p} - a_i),$$

and the aggregate objective over all N observations is

$$E(p) = \sum_{i=1}^{N} \|r_i\|^2 = \sum_{i=1}^{N} \| (I - d_i d_i^\top)(p - a_i) \|^2.$$

Minimizing $E(p)$ yields the normal equations above. The update for $\hat{p}$ in matrix form is obtained by solving

$$\left(\sum_{i=1}^{N} (I - d_i d_i^\top) \right) \hat{p} = \sum_{i=1}^{N} (I - d_i d_i^\top) a_i.$$

If surface normals n_i are known, incident directions refine according to the specular reflection rule

$$r_i = d_i - 2(d_i \cdot n_i) n_i,$$

providing better geometric fidelity for reflective glints.

9.2. Time-of-Arrival and Time-Difference-of-Arrival Constraints

When range or timing information is available, each observation defines a spherical constraint centered at receiver position a_i with radius ct_i, where c is the propagation speed and t_i is the measured travel time. The emitter must satisfy

$$\|\hat{p} - a_i\| = c\, t_i.$$

This nonlinear system can be linearized around an initial estimate $\hat{p}_0$ by substituting a first-order expansion. Define

$$d_i = \frac{\hat{p}_0 - a_i}{\|\hat{p}_0 - a_i\|},$$

and approximate the constraint by its tangent plane:

$$d_i^\top(\hat{p} - a_i) = c\,t_i.$$

For N receivers, the linearized system becomes

$$D\hat{p} = r,$$

where

$$D = \begin{bmatrix} d_1^\top \\ d_2^\top \\ \vdots \\ d_N^\top \end{bmatrix}, \quad r = \begin{bmatrix} c\,t_1 + d_1^\top a_1 \\ c\,t_2 + d_2^\top a_2 \\ \vdots \\ c\,t_N + d_N^\top a_N \end{bmatrix}.$$

This can be incorporated into the least-squares framework by augmenting A and b:

$$A' = A + D^\top D, \quad b' = b + D^\top r.$$

In systems measuring only relative times (TDOA), pairwise subtraction removes the unknown synchronization term δ:

$$(\|\hat{p} - a_i\| - \|\hat{p} - a_j\|) = c\,(t_i - t_j),$$

producing an equivalent overdetermined set of linearized equations solved jointly with ray constraints.

9.3. Phase-Gradient and Polarization Field Analysis

Coherent radar or interferometric receivers can infer propagation directions from phase gradients across their apertures. Let $\phi(x, y)$ denote the measured spatial phase field. The local gradient defines the incident wave direction:

$$d_i = \frac{\nabla\phi(x_i, y_i)}{\|\nabla\phi(x_i, y_i)\|},$$

with the aperture element position serving as a_i. Each sample introduces a residual equation

$$(I - d_i d_i^\top)(\hat{p} - a_i) = 0.$$

Summing across the entire aperture:

$$\sum_{i=1}^{N} (I - d_i d_i^\top)(\hat{p} - a_i) = 0.$$

Polarization measurements provide additional constraints on d_i, enabling correction of multipath interference and improved angular estimation. The weighted least-squares extension is

$$A_w = \sum_{i=1}^{N} w_i (I - d_i d_i^\top), \quad b_w = \sum_{i=1}^{N} w_i (I - d_i d_i^\top) a_i,$$

where w_i are confidence weights derived from coherence or SNR.

9.4. Intensity and Shadow Boundary Inference

In passive optical scenarios, observed illumination and shadow boundaries yield approximate emitter directions. For each illuminated surface with centroid a_i and observed lighting vector l_i, the inferred propagation direction is

$$d_i = -\frac{l_i}{\|l_i\|}.$$

Each patch contributes a constraint enforcing perpendicularity between the vector $(\hat{p} - a_i)$ and the normal projection operator:

$$(I - d_i d_i^\top)(\hat{p} - a_i) = 0.$$

Over N surfaces, the aggregate form becomes

$$\sum_{i=1}^{N} (I - d_i d_i^\top)(\hat{p} - a_i) = 0.$$

This formulation allows emitter localization even from purely visual evidence, provided sufficient directional diversity among illuminated surfaces.

10. Hidden-Emitter Localization from Intermediate Backscatter

Intermediate backscatter provides indirect access to emitter geometry through reflections. An observer at known position o detects a return from x_i, a reflection point within the mapped environment. The hidden emitter $p^\star$ must satisfy the back-projection relation

$$p^\star = x_i - \lambda_i d_i, \quad \lambda_i > 0.$$

If surface normals n_i are known, the valid half-space condition $(x_i - p^\star) \cdot n_i \leq 0$ restricts the emitter to the physically plausible side of the surface. For specular reflection, the incoming, and outgoing directions obey

$$r_i = d_i - 2(d_i \cdot n_i) n_i,$$

where r_i is the unit vector from x_i to the observer. Aggregating all backscatter rays $(a_i = x_i, d_i = \hat{d}_i)$ yields the leastsquares condition

$$\sum_{i=1}^{N} (I - d_i d_i^\top)(p - a_i) = 0.$$

If timing is measured, the total path constraint between emitter, reflection point, and observer is

$$\|p^\star - x_i\| + \|x_i - o\| = c\, t_i + \delta,$$

and the differenced form removing δ is

$$(\|p^\star - x_i\| - \|p^\star - x_j\|) + (\|x_i - o\| - \|x_j - o\|) = c\,(t_i - t_j).$$

These can be merged with the linear system via alternating minimization or Gauss–Newton refinement. Terrain or occlusion models contribute additional feasibility checks through line-of-sight constraints LOS($p^\star$, x_i) = true.

11. Post Hoc Recovery and Real-Time Operations

The same estimator serves both offline and streaming contexts. In post hoc recovery, previously acquired Cartesian point sets are reprocessed to recover missing origin metadata, enabling accurate normal orientation, divergence modeling, and intensity correction. For real-time operation, accumulators are maintained incrementally:

$$A = \sum_{i=1}^{N} P_i, \quad b = \sum_{i=1}^{N} P_i a_i, \quad P_i = (I - d_i d_i^{\top}).$$

At each update step, new observations (a_k, d_k) are incorporated as

$$A_{t+1} = A_t + P_k, \quad b_{t+1} = b_t + P_k a_k,$$

and the updated estimate is

$$\hat{p}_{t+1} = A_{t+1}^{-1} b_{t+1}.$$

Rank-one Sherman–Morrison updates maintain A^{-1} efficiently in streaming form. Weighting terms w_i derived from residuals, timing errors, or coherence metrics improve robustness:

$$A = \sum_{i=1}^{N} w_i P_i, \quad b = \sum_{i=1}^{N} w_i P_i a_i.$$

This formulation supports dynamic targeting, emitter tracking, and sensor geolocation under occlusion.

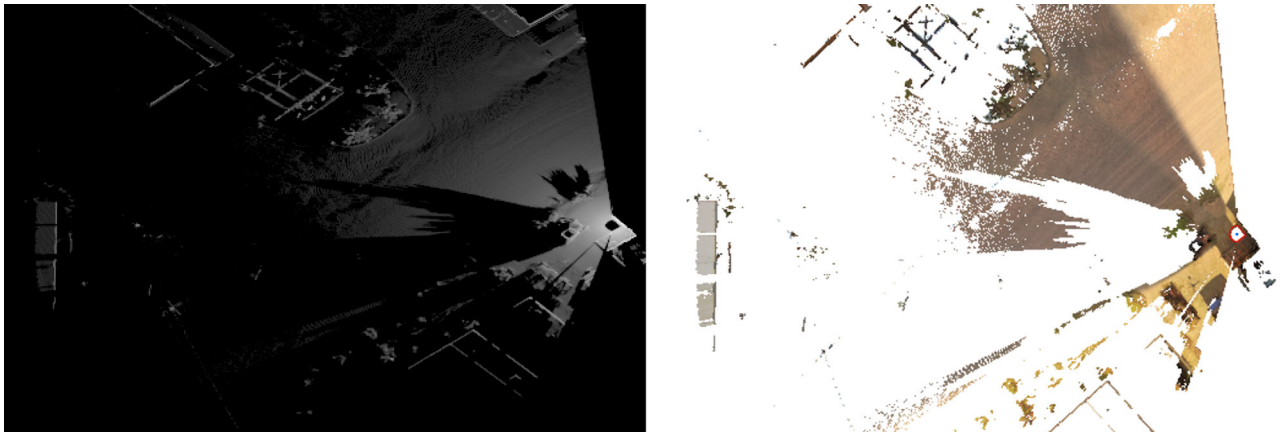

Constrained Source Auto-Circled in Red

12. Comments

The relationships derived above reveal a geometric balance that is present in all polar sensing data. Each observation of position and direction contributes to a spatial equilibrium that exists independent of the sensing system. This balance arises from how rays and observation points are arranged in space. The least-squares intersection does not create this structure, it reveals it. The resulting point marks where all directional evidence is mutually consistent within the geometry already contained in the data.

This equilibrium represents a symmetry between emission and observation. The perpendicular offsets between a test origin and each propagation ray define a residual field that reaches its minimum where the geometry is most coherent. The least-squares process identifies this position by reducing the total residual energy, tracing the system back to the geometric center implied by the data. The same relationship is observed across LiDAR, radar, and sonar data, all of which share a radial structure once expressed in terms of direction and position. The underlying symmetry appears whether the rays correspond to scanlines, reflections, or interference measurements.

In operation, this relationship can be updated continuously as new measurements arrive, maintaining an evolving estimate of the origin as evidence accumulates. Weighted versions of the intersection account for variation in confidence or coherence among observations,

while timing and power-distance information refine the solution through additional constraints. Terrain and occlusion data define the boundaries of this balance, limiting possible origins to those that maintain clear geometric visibility to the observed points [1-9].

Emitter localization reveals the geometric equilibrium that exists within the data rather than creating a model to explain it. The summation form of the least-squares intersection provides a direct way to measure and describe this balance from observed directions and positions across different sensing systems and observation periods. The consistency that emerges reflects the geometry itself, independent of the platform or the method used to collect the measurements.

References

1. Foy, W. H. (2007). Position-location solutions by Taylor-series estimation. *IEEE transactions on aerospace and electronic systems*, (2), 187-194.
2. Kanatani, K., Sugaya, Y., & Niitsuma, H. (2008, September). Triangulation from Two Views Revisited: Hartley-Sturm vs. Optimal Correction. In *BMVC* (pp. 1-10).
3. Hartley, R. I., & Sturm, P. (1997). Triangulation. *Computer vision and image understanding, 68*(2), 146-157.
4. Hartley, R., & Zisserman, A. (2003). *Multiple view geometry in computer vision.* Cambridge university press.
5. Chan, Y. T., & Ho, K. C. (1994). A simple and efficient estimator for hyperbolic location. *IEEE transactions on signal processing, 42*(8), 1905-1915.
6. Nardone, S. C., & Aidala, V. J. (2007). Observability criteria for bearings-only target motion analysis. *IEEE Transactions on Aerospace and Electronic systems,* (2), 162-166.
7. Henry, S., & Christian, J. A. (2023). Absolute triangulation algorithms for space exploration. *Journal of Guidance, Control, and Dynamics, 46*(1), 21-46.
8. Compagnoni, M., Pini, A., Canclini, A., Bestagini, P., Antonacci, F., Tubaro, S., & Sarti, A. (2017). A geometrical–statistical approach to outlier removal for TDOA measurements. *IEEE Transactions on Signal Processing, 65*(15), 3960-3975.
9. Shi, H., Zhang, H., & Wang, X. (2016). A TDOA technique with super-resolution based on the volume cross-correlation function. *IEEE Transactions on Signal Processing, 64*(21), 5682-5695.